APPLIED SCIENCES AND ENGINEERING

A potentiometric mechanotransduction mechanism for novel electronic skins

Xiaodong Wu[1,2], Maruf Ahmed[1], Yasser Khan[1], Margaret E. Payne[1], Juan Zhu[1], Canhui Lu[2]*, James W. Evans[3], Ana C. Arias[1]*

Human skin perceives external mechanical stimuli by sensing the variation in the membrane potential of skin sensory cells. Many scientists have attempted to recreate skin functions and develop electronic skins (e-skins) based on active and passive sensing mechanisms. Inspired by the skin sensory behavior, we investigated materials and electronic devices that allow us to encode mechanical stimuli into potential differences measured between two electrodes, resulting in a potentiometric mechanotransduction mechanism. We present here a potentiometric mechanotransducer that is fabricated through an all-solution processing approach. This mechanotransducer shows ultralow-power consumption, highly tunable sensing behavior, and capability to detect both static and low-frequency dynamic mechanical stimuli. Furthermore, we developed two novel classes of sensing devices, including strain-insensitive sensors and single-electrode-mode e-skins, which are challenging to achieve using the existing methods. This mechanotransduction mechanism has broad impact on robotics, prosthetics, and health care by providing a much improved human-machine interface.

INTRODUCTION

As the largest organ in the human body, skin plays a vital role in mediating our daily interactions with the surrounding environment. With a remarkable network of sensors, human skin can perceive external mechanical stimuli (e.g., touch, pressure, strain, vibration) and encode them into physiological signals that are then interpreted by the brain to form sensory feedback (*1*–*2*). To recreate the properties of human skin, artificial electronic skins (e-skins) have attracted tremendous attention because of their promising applications in robotics, prosthetics, health care, and the Internet of Things (*3*–*4*). In the past decade, notable progress has been made in this field, especially, incorporating features such as high sensitivity (*5*), low detection limit (*6*), biocompatibility (*7*), self-healing capability (*8*–*9*), and good stretchability (*10*–*11*). Looking into these advancements, most of them are realized on the basis of structure engineering (e.g., micropyramids, microcracks, wrinkling, serpentine structures, kirigami structures) and innovations in materials (e.g., nanoparticles, nanowires, two-dimensional materials, conductive polymers, biocompatible and self-healing materials). In addition to these two aspects, innovation in sensing mechanisms is an essential approach to fabricating e-skins with novel properties. Nevertheless, beyond the existing sensing mechanisms (e.g., resistive, capacitive, transistor based, optical, piezoelectric, triboelectric, and piezoionic), sensing mechanism innovation is rarely reported (*2*, *12*–*15*).

In the skin's sensory system (Fig. 1A), cutaneous mechanoreceptors give us the means to perceive external mechanical stimuli via the variation in membrane potential (*16*–*18*). At rest, the inside of the skin sensory cells is usually more negatively charged with respect to the outside (Fig. 1B). When external stimuli are coupled with the sensory cells, the mechanically gated ion channels will be opened, allowing migration or flow of ions across the cell membrane (*16*, *19*). This process produces a large upswing in membrane potential (Fig. 1C, depolarization phase). With the mechanical stimuli released, the membrane potential goes back to the initial level by pumping specific ions back across the cell membrane (Fig. 1C, repolarization phase). This mechanotransduction mechanism via the variation in membrane potential provides a highly effective and energy-efficient way to perceive environmental stimuli.

Inspired by the skin sensory behavior, we present here a potentiometric mechanotransduction mechanism based on mechanically regulated potential difference measured between two electrodes. When bringing two categories of carefully selected electrode materials [Prussian blue–modified graphite carbon (PB/carbon) and silver/silver chloride (Ag/AgCl)] into contact with an electrolyte containing sodium chloride (NaCl), a potential difference is developed between the two electrodes. Via component manipulation of the electrolyte and creating microstructure on the electrolyte surface, the electrolyte/electrode interface can be regulated by external mechanical stimuli, resulting in a variation in the potential difference measured between the two electrodes. Using this strategy, we can encode mechanical stimuli into potential difference variation, similarly to skin sensory cells coupling mechanical stimuli into membrane potential variation. The device reported here, based on this potentiometric mechanotransduction mechanism, does not rely on an external energy source and shows ultralow-power consumption. We recorded less than 1-nW power consumption, which is several orders of magnitude lower than that of conventional sensing devices (*12*). In addition, the fabricated potentiometric mechanotransducer exhibits a good capability to detect both static and low-frequency dynamic mechanical stimuli, compensating for the limitations of self-powered piezoelectric and triboelectric devices in recording static mechanical stimuli (*3*, *20*). Furthermore, we developed an all-solution processing approach to fabricate high-yield potentiometric devices using all commercially available materials, exhibiting good scalability and cost-efficiency.

On the basis of the proposed potentiometric mechanotransduction mechanism, we demonstrate two types of flexible and wearable sensing devices with properties that are challenging to achieve

[1]Department of Electrical Engineering and Computer Sciences, University of California, Berkeley, Berkeley, CA 94720, USA. [2]State Key Laboratory of Polymer Materials Engineering, Polymer Research Institute of Sichuan University, Chengdu 610065, China. [3]Department of Materials Science and Engineering, University of California, Berkeley, Berkeley, CA 94720, USA.
*Corresponding author. Email: acarias@eecs.berkeley.edu (A.C.A.); canhuilu@scu.edu.cn (C.L.)

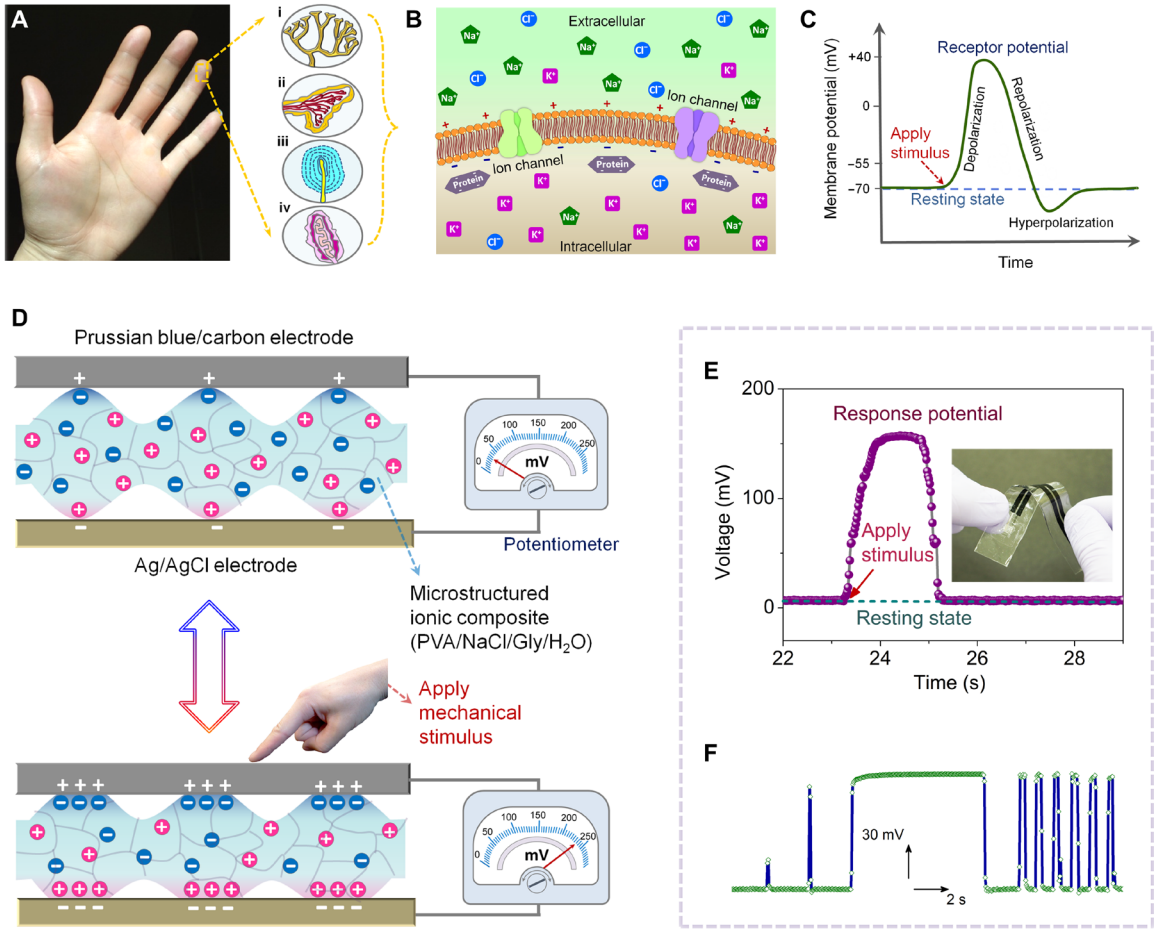

Fig. 1. Potentiometric mechanotransduction mechanism inspired by the skin's sensory behavior. (**A**) Illustrations of the cutaneous mechanoreceptors in natural skin sensory system, including Merkel cells (i), Ruffini endings (ii), Pacinian corpuscles (iii), and Meissner corpuscles (iv). (**B**) Schematic showing the asymmetric ion distribution across the cell membrane, forming a potential difference between the interior and exterior of sensory cells. (**C**) Diagram depicting the membrane potential variation while applying a mechanical stimulus on the sensory cells (depolarization phase) and releasing the mechanical stimulus (repolarization phase). (**D**) Conceptual illustration of the potentiometric mechanotransduction mechanism. Two reversible oxidation-reduction reactions in Prussian blue and Ag/AgCl (as depicted by Eqs. 1 and 2) are used to create a potential difference. Via structural and component manipulation of the electrolyte, the potential difference created between the two electrodes can be gradually altered by applying a force. Thus, external mechanical stimuli can be directly coupled into voltage signal output, just like skin sensory cells coupling mechanical stimuli into membrane potential variation. (**E**) A typical response of the potentiometric sensors when subjected to a mechanical stimulus, which is analogous to the physiological signal generated by the skin sensory cells. (**F**) Response signal of the potentiometric sensors when they are subjected to static and dynamic mechanical stimuli of different magnitudes. Photo credit: X.W., University of California, Berkeley.

via conventional sensing mechanisms. First, we describe a class of soft and stretchable mechanical sensors with strain-independent sensing performance. When the sensors are subjected to tensile deformation up to 50% strain, the signal output of the sensors remains highly stable (nearly no signal variation) during the whole stretching process. This strain-independent sensing performance is rarely reported, since the resistance variation of conventional sensors upon stretching would affect their performance. These strain-insensitive sensors are highly desired for the manufacturing of fully soft, stretchable, and reliable robots and prostheses. Moreover, we demonstrate a type of e-skin with a single-electrode-mode configuration, which shows great performance by enhancing the sensing pixel density and the data acquisition speed compared with traditional dual-electrode-mode e-skins. These distinctive characteristics (summarized in table S1) of the potentiometric mechanotransduction mechanism provide new ways of designing sensors and integrated electronics and contribute to the future development of innovative smart electronic systems.

RESULTS

Design concept of potentiometric mechanotransduction mechanism

To imitate the skin's sensory behavior and establish a potentiometric mechanotransduction mechanism, we first carefully select two active electrode materials (i.e., PB/carbon and Ag/AgCl) that can generate a potential difference. Specifically, for the PB/carbon electrode, there is an oxidation-reduction equilibrium reaction between Fe^{II} and Fe^{III} (Eq. 1, where A is an alkali cation) (*21*). Ag/AgCl is widely used as a reference electrode due to its stable potential, which arises from the oxidation-reduction equilibrium reaction between Ag^0 and Ag^+ in a Cl^- environment (Eq. 2). Combining these two highly reversible

oxidation-reduction equilibrium reactions, a stable potential difference is developed between the two electrodes (fig. S1)

$$AFe^{II}Fe^{III}(CN)_6 + xA^+ + xe^- \leftrightarrow A_{1+x}Fe^{II}[Fe^{II}(CN)_6]_x[Fe^{III}(CN)_6]_{1-x} \quad (1)$$

$$Ag + Cl^- \leftrightarrow AgCl + e^- \quad (2)$$

Once the potential difference is generated, the external mechanical stimuli need to be transduced into a continuous potential difference variation. As shown in fig. S1 (A and B), using ionic solution or ionic hydrogel as an electrolyte, the development of the potential difference between the two electrodes is too fast to control due to the low impedance of these electrolytes, which is measured at the magnitude of kilohms. This low impedance is not high enough to regulate the potential difference output between the two electrodes. To realize a continuous mechanotransduction process, component and structural manipulation of the electrolyte is necessary to effectively regulate the potential difference output between the two electrodes. Through modulating the water content of the electrolyte and creating microstructure on the electrolyte surface (figs. S1C and S2 and Fig. 1D), the potential difference output between the two electrodes could be gradually regulated by an external force (figs. S1C and S3D). The detailed mechanism of this potentiometric mechanotransduction process is fully discussed in the Supplementary Materials (see fig. S3). Via this proposed potentiometric mechanotransduction mechanism, we can successfully encode external mechanical stimuli into continuous potential difference variation, resulting in mechanotransducers with similar signal output with that of natural skin sensory cells (Fig. 1, D and E).

It is worth pointing out that previously reported devices based on piezoelectric and triboelectric effects (*20*, *22*), variation in electrical double layers (*23*), and movement of ions in ionic polymer-metal composites (*24*) can also generate voltage signals in response to external mechanical stimuli. Nevertheless, they selectively respond to dynamic stimuli with transient voltage outputs. Devices that use streaming potential (*25*) can generate voltage signal as well, but a continuous pressure gradient is needed. In contrast, this potentiometric mechanotransduction process enables us to monitor both static and low-frequency dynamic mechanical stimuli of different magnitudes (Fig. 1F), compensating for the limitations of the devices mentioned above. This potentiometric sensing mechanism makes it possible to create novel devices, such as strain-insensitive sensors and single-electrode-mode e-skins, which are challenging to design and fabricate via the conventional sensing principles. The detailed comparison of this potentiometric sensing mechanism with other sensing mechanisms is presented in table S1.

All-solution–based fabrication of potentiometric mechanotransducers

To fabricate the potentiometric mechanotransducers, we first sandwich a microstructured ionic composite between the two electrodes, as illustrated in Fig. 2A. Applying a force upon the mechanotransducers

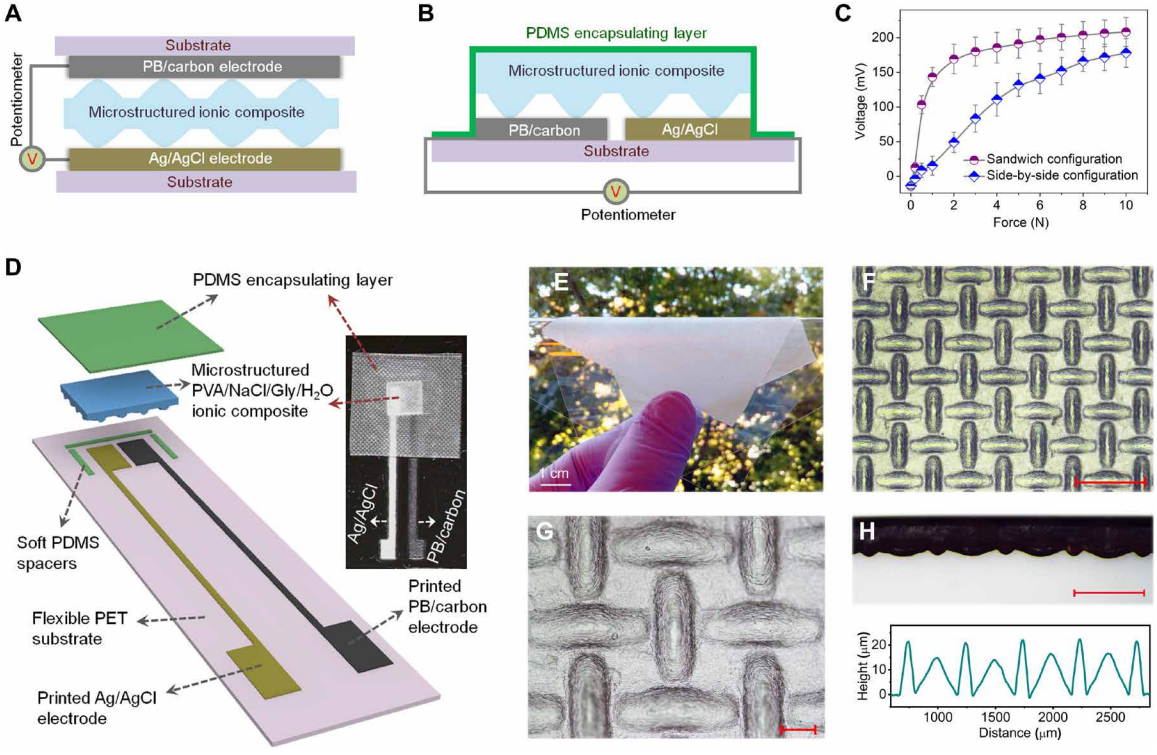

Fig. 2. All-solution–based fabrication of the potentiometric mechanotransducers. (**A** and **B**) Schematic illustrations showing the mechanotransducers with sandwich structure (A) and side-by-side electrode configuration (B). (**C**) Response behaviors of mechanotransducers with different configurations. The contact area of the applied force is ≈16 mm^2. (**D**) Schematic layout and photograph of the potentiometric mechanotransducers fabricated through an all-solution processing approach. See fig. S4 for the fabrication process. (**E**) Picture of a microstructured PVA/NaCl/glycerol (Gly)/water ionic composite film attached on a PET substrate. (**F** and **G**) Optical micrographs showing the created microstructure on the surface of the ionic composite via a mesh-molding strategy. See fig. S5 for the whole process flow. Scale bars, 500 μm (F) and 100 μm (G). (**H**) Cross-sectional morphology and surface profile of the microstructured ionic composite. Scale bar, 500 μm. Photo credit: X.W., University of California, Berkeley.

will simultaneously increase the contact area between the ionic composite and both of the electrodes. A larger force gives rise to a higher potential difference between the two electrodes, as shown in Fig. 2C. Nevertheless, this sandwich structure is not compact as there is no binding between the ionic composite and the electrodes. In addition, it is difficult to encapsulate the mechanotransducers with this sandwich structure. To address these issues, we use a side-by-side electrode configuration with the microstructured ionic composite placed on top of the two electrodes as illustrated in Fig. 2 (B and D). After encapsulation with a soft polydimethylsiloxane (PDMS) layer, the mechanotransducers with the side-by-side electrode configuration are very compact and also easy to construct via continuous and scalable processes. The sensitivity of the side-by-side electrode configuration is lower than that of the sandwich structure (Fig. 2C), but we can compensate for this easily by increasing the water content of the ionic composite (fig. S2). Hence, the side-by-side electrode configuration is used in this study.

We develop an all-solution processing approach to fabricate the potentiometric mechanotransducers (fig. S4). Specifically, commercial PB/carbon ink and Ag/AgCl ink are stencil printed on a flexible polyethylene terephthalate (PET) substrate in sequence, followed by curing the inks into solid electrodes. For the ionic composite, we select eco-friendly polyvinyl alcohol (PVA) as the polymer matrix and sodium chloride (NaCl) as the ion source. In addition, we incorporate nontoxic glycerol (Gly) into the ionic composite. Gly acts as a humectant and can be used to tune the water content and electrical impedance of the ionic composite (fig. S2). Gly also serves as a plasticizer that can increase the softness of the ionic composite. With the synergy of these two aspects, the sensitivity of the potentiometric mechanotransducers can be easily regulated by adjusting the Gly content. The ionic composite is prepared by casting PVA/NaCl/Gly aqueous solutions onto a micropatterned template. After drying, a microstructured PVA/NaCl/Gly/water ionic composite could be obtained (Fig. 2E). A mesh-molding strategy is used to create periodic microstructure on the PVA/NaCl/Gly/water ionic composite (fig. S5). The microstructure created by this mesh-molding strategy is very uniform and periodic, as shown in Fig. 2 (F to H). Last, we integrate the printed electrodes and the ionic composite into compact potentiometric mechanotransducers by encapsulating the devices with a thin PDMS layer (Fig. 2D). Through this eco-friendly, cost-effective, and all-solution processing approach, we can fabricate scalable and high-yield mechanotransducers.

Response behaviors of potentiometric mechanotransducers

The typical response of the potentiometric mechanotransducers when gradually applying a force (the contact area of the applied force is $\approx$16 mm^2) on the devices is shown in Fig. 3A. The smooth increase in voltage signal verifies the capability of the mechanotransducers for continuously monitoring external mechanical stimuli. The response performance of the mechanotransducers can be easily modulated by tuning the Gly content in the PVA/NaCl/Gly/water ionic composite (Fig. 3B). Here, we use a simple equation to evaluate the sensitivity (S) of the mechanotransducers: $S = \Delta V/\Delta F$, where ΔV is the change in voltage output and ΔF is the change in the applied force. As shown in Fig. 3B, mechanotransducers fabricated with the ionic composite of PVA/NaCl/Gly/water-32% exhibit the highest sensitivity of 205.5 mV/N in the force range of 0 to 1 N. Subsequently, the signal variation slows down (2.3 mV/N) in the force range of 1 to 10 N. Mechanotransducers fabricated with the ionic composite of PVA/NaCl/Gly/water-16% show a sensitivity of 48.6 and 3.6 mV/N in the force ranges of 0 to 3 and 3 to 10 N, respectively. For the mechanotransducers fabricated with the ionic composite of PVA/NaCl/Gly/water-8%, the sensitivity tends to be constant, exhibiting 9.5 mV/N in the whole force range. This is because Gly can increase the electrical conductance and the softness of the ionic composites. We can further tune the Gly content in the ionic composites to achieve a higher sensitivity or a broader working range. In addition, the sensing performance of the mechanotransducers can be regulated by tuning the microstructure size of the ionic composites (fig. S6), which further enhances the tunability of the devices. The mechanotransducers also exhibit fast response and recovery behavior, with the response and recovery time measured to be $\approx$71 and $\approx$106 ms, respectively (Fig. 3C).

As shown in Fig. 3D, when a static force is applied on the mechanotransducers and maintained for 50 s, the recorded voltage signal keeps nearly constant during this period. Piezoelectric and triboelectric sensing devices can also generate voltage signal output, but they cannot be used to record static or slowly varying mechanical stimuli. This potentiometric mechanotransduction mechanism provides a new methodology for continuous monitoring of static or slowly varying mechanical stimuli with self-generated voltage output (Fig. 3, A and D), compensating for the limitation of piezoelectric and triboelectric sensing devices in this regard. Besides, the potentiometric mechanotransducers are capable of detecting low-frequency dynamic mechanical stimuli from 0.5 to 2 Hz, as shown in Fig. 3E. These mechanotransducers also exhibit desirable durability in a cyclic test (Fig. 3F) and desirable sensing capability in a long-term continuous operation under ambient condition (fig. S7A). Nevertheless, these devices are not suitable for use at high temperature, as high temperature can break the steady state of the sensor system (fig. S7B). Notably, the power consumption of our potentiometric devices is ultralow and recorded less than 1 nW during the potentiometric measurement, which is several orders of magnitude lower than that of conventional sensing devices. This is because the measured potential difference between the two electrodes is self-generated and does not rely on an external power supply. These energy-saving devices are highly desirable for large-scale sensing systems.

Strain-insensitive mechanical sensors

Compared with flexibility, stretchability will be a more desired characteristic for the next generation of electronic devices as it can improve the deformability, conformability, and robustness of electronic components (*26*). However, developing stretchable mechanical sensors still remains a great challenge because mechanical stimuli cannot be measured independently from stretching-induced interference. Intrinsically stretchable conductive materials (*10*–*11*, *27*) are expected to exhibit small conductance change under stretching and can be used to alleviate this issue. However, complicated chemical synthesis or elaborate microphase manipulations are generally needed, and it is still difficult to eliminate the stretching-induced interference completely. Recently, structure engineering of unstretchable materials and devices (e.g., serpentine structures, waving structures, kirigami structures) shows good promise to fabricate stretchable electronics (*28*–*33*). Nevertheless, this strategy usually involves sophisticated fabrication processes and is also disadvantageous for high-density device integration. These aspects limit their practical and widespread application. Therefore, developing a facile and scalable approach to create mechanical sensors with strain-independent

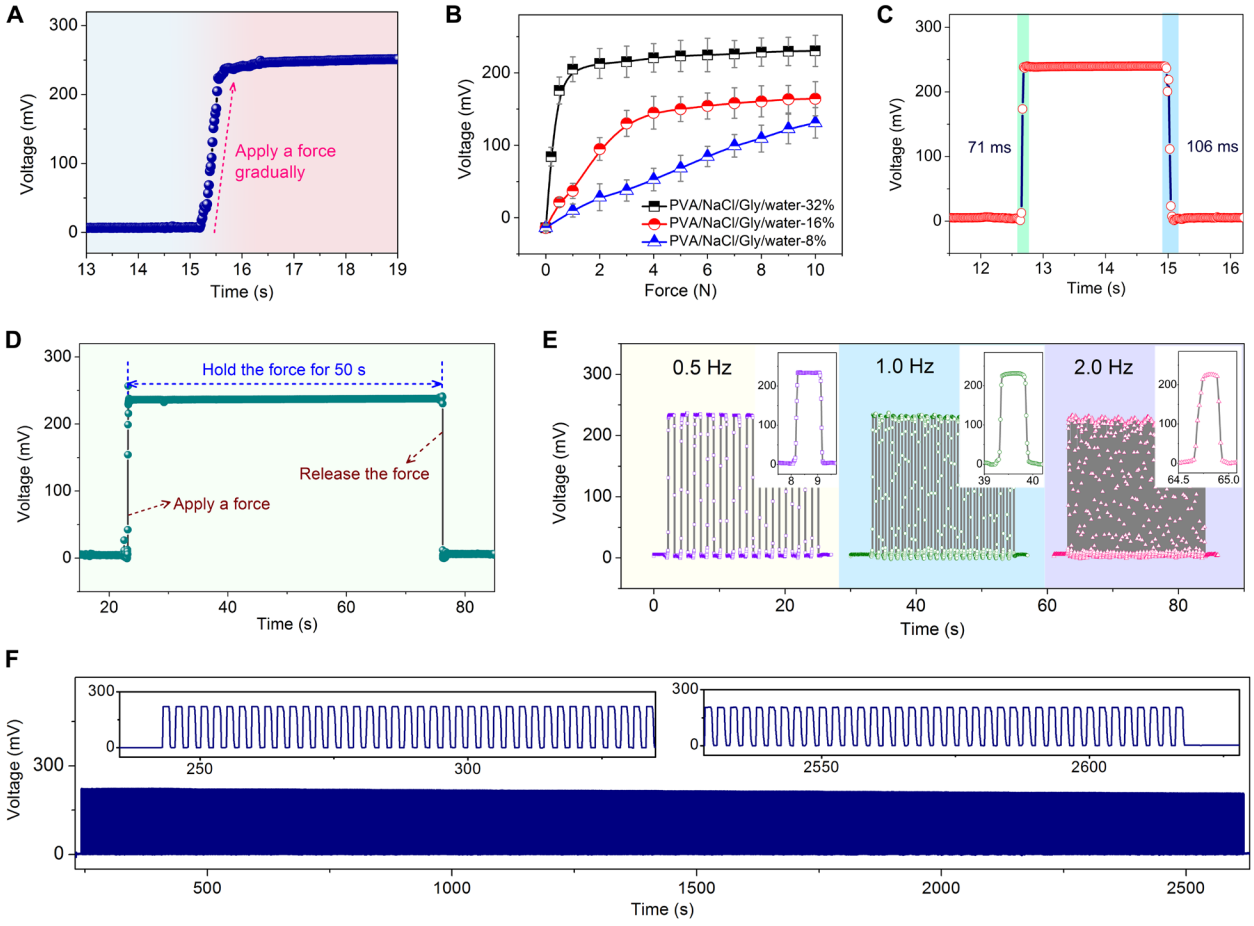

Fig. 3. Response behaviors of the potentiometric mechanotransducers. (**A**) Recorded voltage signal of a mechanotransducer while gradually applying a force on the device, showing a continuous and smooth mechanotransduction behavior. (**B**) Response behaviors of mechanotransducers with ionic composites of different Gly content. PVA/NaCl/Gly/water-*X*% signifies that the weight ratio of Gly:PVA is *X*%. Gly enables efficient regulation of the electrical impedance and the softness of the ionic composites and thus can tune the sensing behavior of the mechanotransducers. Ionic composite of PVA/NaCl/Gly/water-32% is used to fabricate mechanotransducers unless otherwise specified. (**C**) Response and recovery behaviors of the mechanotransducer. (**D**) Recorded voltage signal of the mechanotransducer while applying a static force on the device for 50 s. The voltage signal under the static force is nearly constant, verifying the ability of the mechanotransducer to record static mechanical stimuli. (**E**) Voltage signal variation of the mechanotransducer when applying a dynamic force (0.5, 1.0, and 2.0 Hz, respectively) on the device, indicating the capability to monitor low-frequency dynamic stimuli. (**F**) Reliability test of the mechanotransducer by loading and unloading a force on the device for 1000 cycles.

sensing behaviors still remains a great challenge but an exciting goal for creating stretchable electronic systems.

In this work, instead of structure or material innovations, we propose a new sensing mechanism (i.e., potentiometric mechanotransduction) to fabricate strain-insensitive mechanical sensors by combining the potentiometric mechanotransducers with elastic conductors. The operating principle of the stretchable sensors is illustrated in Fig. 4A. In principle, the potential difference between the two electrodes is measured as an open-circuit potential. For the open-circuit potential measurement, a huge resistor (R_∞) is connected with the circuit, and the voltage measurement is performed across R_∞. This setup ensures the generated voltage in the sensors drops primarily across R_∞. During stretching deformation, the resistance variation of the elastic conductors (R_1) can be neglected in comparison with the R_∞ and will not cause an impact on the overall resistance of the entire circuit loop. Hence, these potentiometric mechanical sensors can work independently from stretching deformation.

The design layout of the stretchable sensors is shown in Fig. 4B, and the fabrication process is illustrated in fig. S8. The fabricated sensors exhibit good softness, flexibility, and stretchability, as presented in Fig. 4C and fig. S9. In the following, the strain insensitivity of the stretchable mechanical sensors is systematically investigated. Because there are two critical factors (i.e., the applied force on the sensors and the stretching deformation of the sensors) during characterizing the strain insensitivity and it is difficult to vary the applied force and the applied strain simultaneously, we need to fix one parameter and vary the other one to evaluate the independence between them.

First, by fixing a force on the sensors and then varying the applied strain, we investigated the effect of stretching interference on the stability of the sensor signal output (fig. S10A). As shown in Fig. 4D, we first apply a constant force on the sensors to generate a signal output (phase i). Then, the sensors are gradually stretched to 50% strain (phase ii), followed by releasing the strain (phase iii). As shown in fig. S10C, during stretching the sensors to 50% strain, the resistance of the elastic conductors increases remarkably, exhibiting a relative resistance change of 31.0%. However, the measured voltage signal of the potentiometric sensors keeps highly stable with nearly

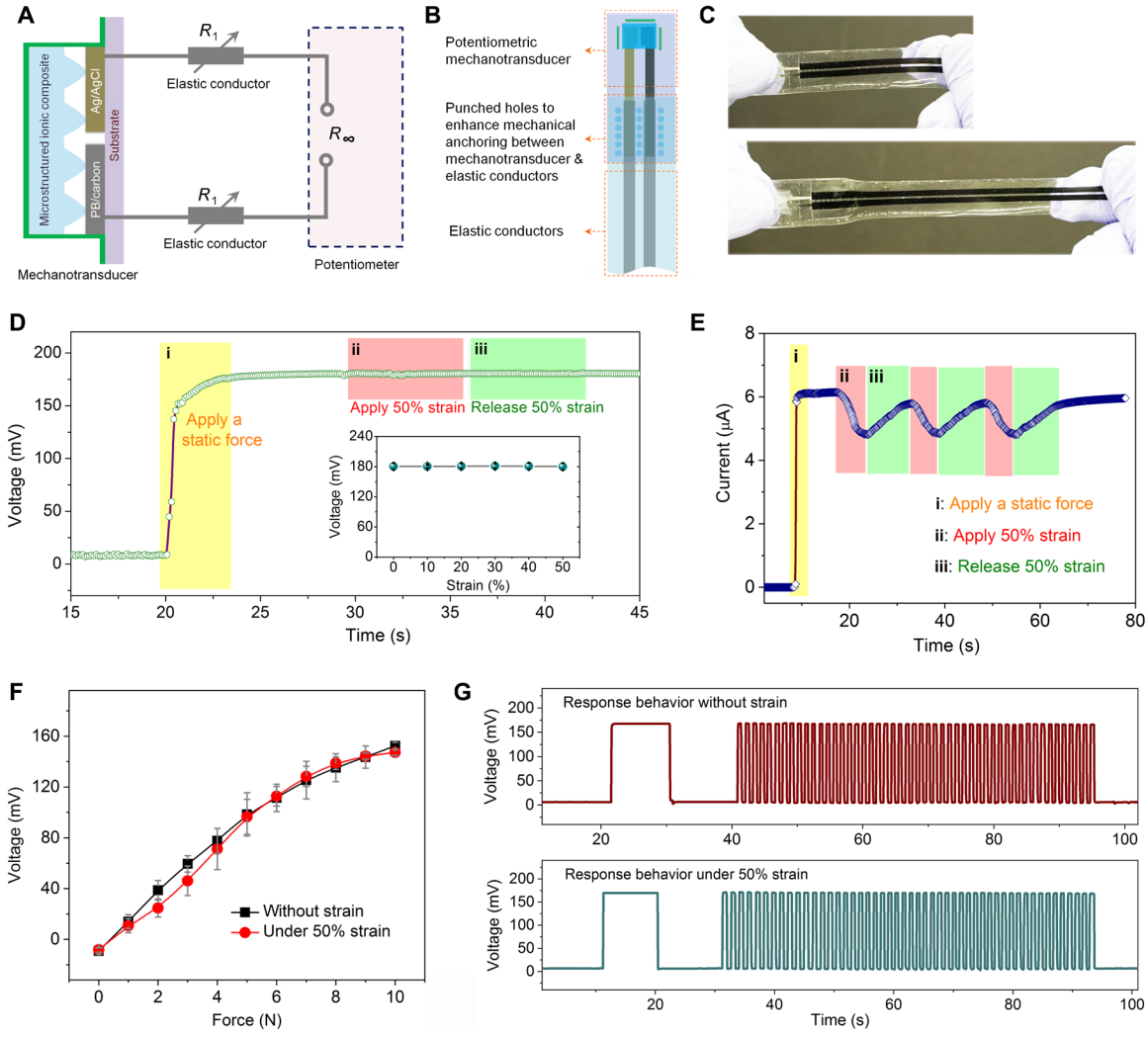

Fig. 4. Stretchable mechanical sensors with strain-independent sensing performance. (**A**) Schematic diagram showing the circuit model for the operating principle of the strain-insensitive potentiometric sensors. (**B**) Illustrative layout of the stretchable sensors. See fig. S8 for fabrication flow. (**C**) Photographs showing the good stretchability of the sensors. (**D**) Recorded voltage signal of a stretchable potentiometric sensor during first applying a constant force onto the sensor (phase i), followed by applying (phase ii) and releasing (phase iii) 50% strain to the sensor. The inset figure shows the highly stable signal output of the sensor during stretching the sensor to 50% strain. See movie S1 for real-time demonstration. (**E**) Measured current signal of a stretchable resistive sensor for comparison. The current signal shows a notable variation during applying/releasing 50% strain as a result of the strain-induced interference. (**F**) Force sensing behaviors of the stretchable sensor without strain and with 50% strain applied on the sensor. (**G**) Response behaviors of a stretchable sensor for monitoring finger touch: without strain and with 50% strain applied on the sensor. The measured signals of the prestretched and unstretched sensors are nearly identical, demonstrating that the sensor can work independently from stretching-induced interference. Photo credit: X.W., University of California, Berkeley.

no signal variation (only ≈0.56% relative signal change; Fig. 4D, inset), exhibiting a strain-independent sensing behavior (see movie S1 for real-time demonstration). As a comparison experiment, we replaced the potentiometric mechanotransducer with a resistive mechanotransducer and kept all other components the same (as described in fig. S11), thus fabricating a stretchable resistive sensor. As shown in Fig. 4E, when the resistive sensor is subjected to stretching (phase ii) and releasing (phase iii) processes, the detected signal exhibits a prominent variation (≈21.3% relative change).

On the other hand, by preapplying a strain on the sensors and then varying the applied force, we investigated the force sensing behaviors of the sensors under different strains (fig. S10B). As shown in Fig. 4F, with 0% strain and 50% strain preapplied on the sensors, the force sensing behaviors are similar to each other, indicating that the preapplied 50% strain on the sensors does not affect their sensing performance. All these data mentioned above verify the advantage of the potentiometric mechanotransduction mechanism for constructing strain-insensitive mechanical sensors.

As a proof of concept, we demonstrate the application of our stretchable sensors for perceiving finger touch independently from stretching-induced interference. First, a finger is pressed onto a tactile sensor and held for ≈10 s to apply a static force. Subsequently, the finger repeatedly presses the tactile sensor for 50 cycles to apply a dynamic force. As shown in Fig. 4G, the potentiometric tactile sensor before and after stretching to 50% strain can detect both static and dynamic stimuli. The prestretched sensor (to 50% strain) and the

unstretched sensor (0% strain) generate nearly identical signals (including signal intensity and signal pattern). This strain-independent sensing capability for both static and dynamic stimulus detection is difficult to realize using conventional sensing mechanisms. We envision that these strain-insensitive sensors are very promising for manufacturing soft robotics, stretchable prosthetics, and comfortable health care devices.

Single-electrode-mode e-skin

For most of the reported e-skins, each sensing pixel usually has two electrodes, so there must be two connection wires for each pixel to acquire and transfer data (Fig. 5A). On the basis of state-of-the-art fabrication techniques, the spatial arrangement of the massive wires limits the pixel density and pixel number of these dual-electrode-mode e-skins. Alternatively, crossed-grid electrode configuration is used to reduce the complexity of the wiring and to improve the pixel density (Fig. 5B) (*34*–*36*). However, the sensing pixels need to be operated one by one to avoid the cross-talk between adjacent pixels, which limits the data acquisition speed. Here, we describe a single-electrode-mode e-skin based on potentiometric mechanotransduction mechanism. Primarily, we use a single electrode as a reference point and measure the potential difference of other sensing electrodes with respect to this reference point (as illustrated in Fig. 5C). There are several advantages for this single-electrode-mode e-skin (see table S2 for detailed comparison). First, this electrode configuration can reduce the complexity of wiring and improve the pixel density compared with dual-electrode-mode e-skins. Second, because there is negligible current flow involved in the potentiometric measurement, the interference and cross-talk between different sensing pixels can be minimized or eliminated. This makes it feasible to acquire data from all of the sensing pixels simultaneously (as demonstrated in fig. S12), which could greatly enhance the data acquisition speed of future e-skins. Moreover, this potentiometric e-skin shows advantage over the other two electrode configurations regarding power consumption (less than 1 nW), which makes it very competitive for practical applications.

The fabrication of the single-electrode-mode e-skins is more economical compared with dual-electrode-mode e-skins. Only three steps are needed: (i) printing of electrode patterns on a flexible substrate, (ii) solution casting of ionic composite film, and (iii) final assembly of the e-skins. As a demonstration, a flexible single-electrode-mode e-skin with 6 × 6 sensing pixels is fabricated (Fig. 5, D and E). The pattern and size of the e-skin can be well defined during the electrode printing procedure. To evaluate the sensing behaviors of the e-skin, a plasticine ball (0.8 g) and a battery (11.0 g) are placed on the 3^{row}-3^{column} pixel (Fig. 5, F and G). The heavier object gives rise to a larger potential difference between this pixel and the reference electrode, revealing good capability for differentiating the magnitude of the applied force. In addition, we arrange steel balls (≈1.0 g) into the shapes of "C," "A," and "L" on the e-skin and measure the potential difference of each pixel with respect to the reference electrodes, as shown in Fig. 5H. The reconstructed color mapping is consistent with the distribution of the objects, demonstrating the capability of the e-skin in resolving spatial pressure distribution. With the merits of facile fabrication, ultralow-power consumption, and good capability of enhancing the pixel density and data acquisition speed, these single-electrode-mode e-skins are very appealing for a wide range of applications, such as flexible touch panels, smart robots, interactive wearable devices, etc.

DISCUSSION

In summary, we have demonstrated a potentiometric mechanotransduction mechanism inspired by the skin's sensory behavior. The potentiometric mechanotransducers fabricated via an all-solution processing approach exhibit ultralow-power consumption (less than 1 nW), high tunability, and a good capability to detect both static and low-frequency dynamic mechanical stimuli. On the basis of this potentiometric sensing mechanism, we report two classes of novel devices: (i) stretchable mechanical sensors with strain-independent sensing performance and (ii) single-electrode-mode e-skins with improved pixel density and data acquisition speed compared with traditional dual-electrode-mode e-skins. As a paradigm of mechanism innovation for mechanotransduction, there are still many aspects that need to be explored. For instance, developing new material systems is necessary for further improving the performance of the mechanotransducers, e.g., response/recovery speed, detectable frequency range. On the other hand, beyond the strain-insensitive sensors and single-electrode-mode e-skins, new electronic devices with other novel properties can be explored. We believe that this work can serve as a stepping stone for realizing soft, stretchable, and multifunctional e-skins of the future.

MATERIALS AND METHODS

All-solution processing fabrication of potentiometric mechanotransducers

PET films (125 μm thick) were used as the substrate for stencil printing of electrode patterns. Kapton tape (60 μm in thickness) films were cut into defined patterns with a laser-cutting machine and attached to the PET substrate as stencils. PB/carbon ink (C2070424P2, Gwent Electronic Materials Ltd.) was first stencil printed as one electrode using a glass slide, followed by drying at 100°C for 10 min. Then, Ag/AgCl ink (CI-4001, Engineered Materials Systems Inc.) was stencil printed as another electrode, followed by curing at 130°C for 1 hour. After removing the Kapton tape stencil, PB/carbon and Ag/AgCl electrodes with defined patterns were formed on the PET substrate. Subsequently, the surface of PB/carbon and Ag/AgCl electrodes was polished with soft and flexible wiping papers (TechniCloth, Texwipe Company) to remove the additives of the inks left on the surface, thus obtaining a more stable electrode surface.

The microstructured PVA/NaCl/Gly/water ionic composites were prepared on the basis of a solution casting method. Specifically, PVA/NaCl/Gly aqueous solutions containing 25 weight % (wt %) PVA, 100 mM NaCl, and Gly (weight ratios of Gly to PVA were 8, 16, and 32%, respectively) were cast on a template with periodic microstructure molded from screen meshes (as described in fig. S5). The cast PVA/NaCl/Gly solutions were first dried in a fume hood at ambient temperature for 24 hours and then dried at an environmental chamber at 25°C and 50% relative humidity (RH) for another 8 hours. After drying, the PVA/NaCl/Gly/water ionic composite films (≈700 μm in thickness) were peeled off from the template and cut into defined shape and size. Subsequently, three PDMS spacers ($0.15 \times 1 \times 5$ mm^3) were placed around the sensing region of the electrodes, and the obtained PVA/NaCl/Gly/water ionic composites were put at the sensing region (as described in fig. S4). Then, the whole mechanotransducers were encapsulated with a thin PDMS layer (≈200 μm in thickness). The outside surface of the encapsulating PDMS layer is microstructured to avoid adhering between the PDMS layer and external objects.

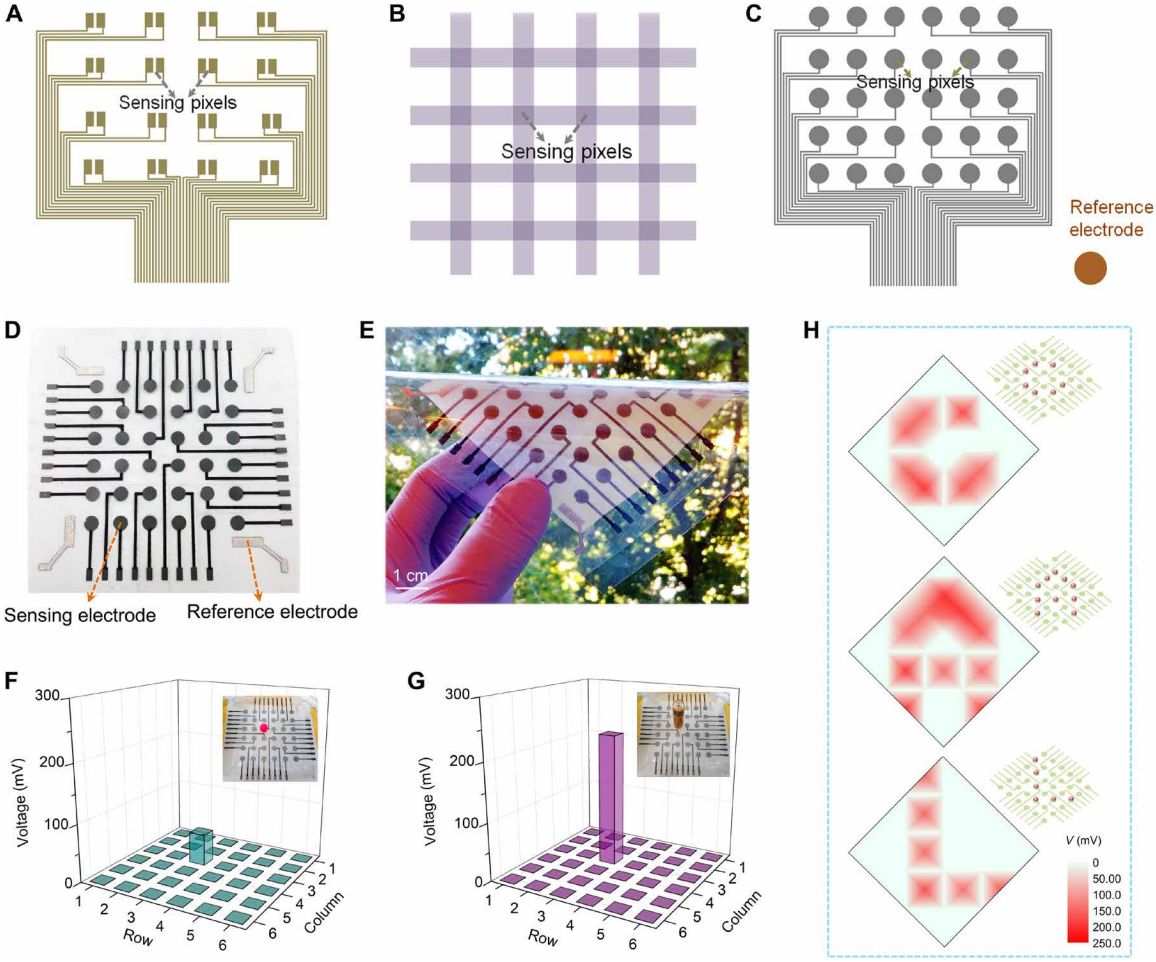

Fig. 5. Single-electrode-mode e-skin. (**A** to **C**) Electrode configurations for e-skin fabrication: dual-electrode mode (A), crossed-grid electrode mode (B), and single-electrode mode (C). (**D**) Photograph showing the printed electrode pattern for fabricating single-electrode-mode e-skin with 6 × 6 sensing pixels. Four reference electrodes are set at the four corners of the e-skin, making each sensing pixel has a similar distance to the reference electrodes. During measurement, the four reference electrodes are connected with one another, forming just one reference point. (**E**) Photograph of a flexible single-electrode-mode e-skin. (**F** and **G**) Response behaviors of the e-skin when placing a plasticine ball of ≈0.8 g (the contact area is ≈8.0 mm^2) and a battery of ≈11.0 g (the contact area is ≈26.4 mm^2) on the 3^{row}-3^{column} pixel, respectively. (**H**) Schematics and spatial mappings in the potential difference of each pixel with respect to the reference electrodes when steel balls (≈1.0 g) are placed on the e-skin, forming the letters "C," "A," and "L" (the logo letters of our university). From the reconstructed color mappings, the letters "C," "A," and "L" could be easily recognized, revealing the desirable pressure mapping capability of the single-electrode-mode e-skin. Photo credit: X.W., University of California, Berkeley.

For potentiometric mechanotransducers with sandwich structure, PVA/NaCl/Gly solution glue was pasted on the unstructured side of two pieces of ionic composite films, followed by bonding them together with the microstructured surface outside. After drying the glue in an environmental chamber (25°C and 50% RH) for 2 hours, the ionic composite film with microstructure on both sides was sandwiched between the PB/carbon and Ag/AgCl electrodes, and a potentiometric mechanotransducer with sandwich structure was fabricated.

Fabrication of stretchable sensors with strain-independent performance

Fabrication of the stretchable sensors contains three major steps. The first step is to fabricate PDMS/carbon nanotubes (CNTs) elastic conductors, as illustrated in fig. S8. Kapton tape mask was attached onto a glass slide to define the conductive patterns, followed by spray coating CNT suspension (25 ml; suspended in alcohol with 1 mg/ml) on the glass slide. After removing the Kapton tape mask, the PDMS precursor (the weight ratio of base to cross-linker is 10:1) was cast onto the glass slide and cured at 100°C for 30 min. Then, the PDMS/CNT elastic conductors were peeled off, with dense CNT conductive network imbedded in the PDMS surface. The second step is to fabricate flexible PB/carbon and Ag/AgCl electrodes on a thin PET substrate (75 μm) based on the procedure mentioned above. Three columns of holes (1 mm in diameter) were punched on the substrate near the electrodes. These holes can mechanically anchor the flexible electrodes and the elastic conductors via the permeated PDMS in the holes after the final assembly process. The third step is the final assembly of the stretchable sensors. First, conductive carbon paste (112-48, Creative Materials Inc.) was pasted on the PB/carbon and Ag/AgCl electrodes near the punched holes. Then, PDMS/CNT elastic conductors were aligned and attached to the electrodes, followed by curing the carbon paste at 100°C for 30 min. Subsequently, PDMS spacers, PVA/NaCl/Gly/water ionic composite (PVA/NaCl/Gly/water-16%), and encapsulating PDMS layer were placed on the

sensing region. Then, the PDMS precursor was dropped into the holes on the substrate, and the whole sensor was sandwiched between two half-cured and sticky PDMS films (prepared by curing PDMS precursor on a hotplate at 100°C for ≈3 min), followed by completely curing the device at 25°C for 48 hours (50% RH). Thus, a soft, flexible, stretchable, and robust mechanical sensor with strain-independent sensing performance was fabricated.

Construction of single-electrode-mode e-skins

The fabrication of the single-electrode-mode e-skin is shown in fig. S13. PB/carbon and Ag/AgCl inks were stencil printed on the substrate, respectively, based on the procedure mentioned above. After drying the inks and removing the stencil, electrodes with defined patterns were obtained. Then, polyvinyl butyral solution (10 wt %, dissolved in ethanol) was drop cast on the conductive trace and dried (acting as an insulating layer), followed by placing 26 PDMS spacers ($0.15 \times 1 \times 5$ mm^3) between adjacent electrodes (as shown in fig. S13). Subsequently, the PVA/NaCl/Gly solution (weight ratio of Gly to PVA is 32%) was pasted onto the Ag/AgCl electrodes as glue, and a piece of microstructured PVA/NaCl/Gly/water ionic composite (65 mm by 65 mm, weight ratio of Gly to PVA is 32%) was placed on the electrodes, with the ionic composite firmly bonded on Ag/AgCl electrodes after drying the glue. Last, a thin PDMS film (150 μm) was put on the e-skin for encapsulation.

Characterization and measurement

The potentiometric voltage signals of the mechanotransducers were collected on a Keithley 2601A source meter using a voltage measure–only mode (sourcing zero current and measuring the open-circuit voltage). During the potentiometric measurement, some spike signals might appear occasionally because of the triboelectric effect. However, these interferential spike signals can be easily filtered, as discussed in fig. S14. Optical microscopic observation was conducted on an optical microscope (Eclipse 50i, Nikon). A Dektak profiler (Veeco 6M) was used for the profile measurement of the microstructured PVA/NaCl/Gly/water ionic composite. Force measurement was conducted on a laboratory-built setup based on a computer-controlled movable stage and a force gauge (M5, Mark-10).

SUPPLEMENTARY MATERIALS

Supplementary material for this article is available at http://advances.sciencemag.org/cgi/content/full/6/30/eaba1062/DC1

REFERENCES AND NOTES

1. H.-H. Chou, A. Nguyen, A. Chortos, J. W. F. To, C. Lu, J. Mei, T. Kurosawa, W.-G. Bae, J. B.-H. Tok, Z. Bao, A chameleon-inspired stretchable electronic skin with interactive colour changing controlled by tactile sensing. *Nat. Commun.* **6**, 8011 (2015).
2. Y. Wu, Y. Liu, Y. Zhou, Q. Man, C. Hu, W. Asghar, F. Li, Z. Yu, J. Shang, G. Liu, M. Liao, R.-W. Li, A skin-inspired tactile sensor for smart prosthetics. *Sci. Robot.* **3**, eaat0429 (2018).
3. A. Chortos, J. Liu, Z. Bao, Pursuing prosthetic electronic skin. *Nat. Mater.* **15**, 937–950 (2016).
4. X. Wang, L. Dong, H. Zhang, R. Yu, C. Pan, Z. L. Wang, Recent progress in electronic skin. *Adv. Sci.* **2**, 1500169 (2015).
5. Z. Wang, S. Guo, H. Li, B. Wang, Y. Sun, Z. Xu, X. Chen, K. Wu, X. Zhang, F. Xing, L. Li, W. Hu, The semiconductor/conductor interface piezoresistive effect in an organic transistor for highly sensitive pressure sensors. *Adv. Mater.* **31**, e1805630 (2018).
6. Y. Zang, F. Zhang, D. Huang, X. Gao, C.-a. Di, D. Zhu, Flexible suspended gate organic thin-film transistors for ultra-sensitive pressure detection. *Nat. Commun.* **6**, 6269 (2015).
7. C. M. Boutry, Y. Kaizawa, B. C. Schroeder, A. Chortos, A. Legrand, Z. Wang, J. Chang, P. Fox, Z. Bao, A stretchable and biodegradable strain and pressure sensor for orthopaedic application. *Nat. Electron.* **1**, 314–321 (2018).
8. Z. Zou, C. Zhu, Y. Li, X. Lei, W. Zhang, J. Xiao, Rehealable, fully recyclable, and malleable electronic skin enabled by dynamic covalent thermoset nanocomposite. *Sci. Adv.* **4**, eaaq0508 (2018).
9. Y. Cao, Y. J. Tan, S. Li, W. W. Lee, H. Guo, Y. Cai, C. Wang, B. C.-K. Tee, Self-healing electronic skins for aquatic environments. *Nat. Electron.* **2**, 75–82 (2019).
10. S. Wang, J. Xu, W. Wang, G.-J. N. Wang, R. Rastak, F. Molina-Lopez, J. W. Chung, S. Niu, V. R. Feig, J. Lopez, T. Lei, S.-K. Kwon, Y. Kim, A. M. Foudeh, A. Ehrlich, A. Gasperini, Y. Yun, B. Murmann, J. B.-H. Tok, Z. Bao, Skin electronics from scalable fabrication of an intrinsically stretchable transistor array. *Nature* **555**, 83–88 (2018).
11. J. Xu, S. Wang, G.-J. N. Wang, C. Zhu, S. Luo, L. Jin, X. Gu, S. Chen, V. R. Feig, J. W. F. To, S. Rondeau-Gagné, J. Park, B. C. Schroeder, C. Lu, J. Y. Oh, Y. Wang, Y.-H. Kim, H. Yan, R. Sinclair, D. Zhou, G. Xue, B. Murmann, C. Linder, W. Cai, J. B.-H. Tok, J. W. Chung, Z. Bao, Highly stretchable polymer semiconductor films through the nanoconfinement effect. *Science* **355**, 59–64 (2017).
12. K.-Y. Chun, Y. J. Son, E.-S. Jeon, S. Lee, C.-S. Han, A self-powered sensor mimicking slow- and fast-adapting cutaneous mechanoreceptors. *Adv. Mater.* **30**, e1706299 (2018).
13. G. S. Cañón Bermúdez, D. D. Karnaushenko, D. Karnaushenko, A. Lebanov, L. Bischoff, M. Kaltenbrunner, J. Fassbender, O. G. Schmidt, D. Makarov, Magnetosensitive e-skins with directional perception for augmented reality. *Sci. Adv.* **4**, eaao2623 (2018).
14. G. S. Cañón Bermúdez, H. Fuchs, L. Bischoff, J. Fassbender, D. Makarov, Electronic-skin compasses for geomagnetic field-driven artificial magnetoreception and interactive electronics. *Nat. Electron.* **1**, 589–595 (2018).
15. C.-C. Kim, H.-H. Lee, K. H. Oh, J.-Y. Sun, Highly stretchable, transparent ionic touch panel. *Science* **353**, 682–687 (2016).
16. N. Sperelakis, *Cell Physiology Source Book* (Academic Press, ed. 4, 2012). chap. 36, pp. 633–647.
17. R. Ikeda, M. Cha, J. Ling, Z. Jia, D. Coyle, J. G. Gu, Merkel cells transduce and encode tactile stimuli to drive Aβ-afferent impulses. *Cell* **157**, 664–675 (2014).
18. M. L. Jin, S. Park, Y. Lee, J. H. Lee, J. Chung, J. S. Kim, J.-S. Kim, S. Y. Kim, E. Jee, D. W. Kim, J. W. Chung, S. G. Lee, D. Choi, H.-T. Jung, D. H. Kim, An ultrasensitive, visco-poroelastic artificial mechanotransducer skin inspired by piezo2 protein in mammalian merkel cells. *Adv. Mater.* **29**, 1605973 (2017).
19. C. Hammond, *Cellular and Molecular Neurophysiology* (Academic Press, ed. 4, 2015). chap. 3, pp. 39–54.
20. J. Park, Y. Lee, M. Ha, S. Cho, H. Ko, Micro/nanostructured surfaces for self-powered and multifunctional electronic skins. *J. Mater. Chem. B* **4**, 2999–3018 (2016).
21. X. Xie, M. Ye, C. Liu, P.-C. Hsu, C. S. Criddle, Y. Cui, Use of low cost and easily regenerated Prussian Blue cathodes for efficient electrical energy recovery in a microbial battery. *Energ. Environ. Sci.* **8**, 546–551 (2015).
22. Z. L. Wang, J. Chen, L. Lin, Progress in triboelectric nanogenerators as a new energy technology and self-powered sensors. *Energ. Environ. Sci.* **8**, 2250–2282 (2015).
23. J. K. Moon, J. Jeong, D. Lee, H. K. Pak, Electrical power generation by mechanically modulating electrical double layers. *Nat. Commun.* **4**, 1487 (2013).
24. J. Zhao, S. Han, Y. Yang, R. Fu, Y. Ming, C. Lu, H. Liu, H. Gu, W. Chen, Passive and space-discriminative ionic sensors based on durable nanocomposite electrodes toward sign language recognition. *ACS Nano* **11**, 8590–8599 (2017).
25. F. H. J. van der Heyden, D. J. Bonthuis, D. Stein, C. Meyer, C. Dekker, Power generation by pressure-driven transport of ions in nanofluidic channels. *Nano Lett.* **7**, 1022–1025 (2007).
26. Z. Huang, Y. Hao, Y. Li, H. Hu, C. Wang, A. Nomoto, T. Pan, Y. Gu, Y. Chen, T. Zhang, W. Li, Y. Lei, N. Kim, C. Wang, L. Zhang, J. W. Ward, A. Maralani, X. Li, M. F. Durstock, A. Pisano, Y. Lin, S. Xu, Three-dimensional integrated stretchable electronics. *Nat. Electron.* **1**, 473–480 (2018).
27. K. Sim, Z. Rao, H.-J. Kim, A. Thukral, H. Shim, C. Yu, Fully rubbery integrated electronics from high effective mobility intrinsically stretchable semiconductors. *Sci. Adv.* **5**, eaav5749 (2019).
28. C. Dagdeviren, Y. Shi, P. Joe, R. Ghaffari, G. Balooch, K. Usgaonkar, O. Gur, P. L. Tran, J. R. Crosby, M. Meyer, Y. Su, R. Chad Webb, A. S. Tedesco, M. J. Slepian, Y. Huang, J. A. Rogers, Conformal piezoelectric systems for clinical and experimental characterization of soft tissue biomechanics. *Nat. Mater.* **14**, 728–736 (2015).
29. S. Xu, Z. Yan, K.-I. Jang, W. Huang, H. Fu, J. Kim, Z. Wei, M. Flavin, J. McCracken, R. Wang, A. Badea, Y. Liu, D. Xiao, G. Zhou, J. Lee, H. U. Chung, H. Cheng, W. Ren, A. Banks, X. Li, U. Paik, R. G. Nuzzo, Y. Huang, Y. Zhang, J. A. Rogers, Assembly of micro/nanomaterials into complex, three-dimensional architectures by compressive buckling. *Science* **347**, 154–159 (2015).
30. S. Xu, Y. Zhang, J. Cho, J. Lee, X. Huang, L. Jia, J. A. Fan, Y. Su, J. Su, H. Zhang, H. Cheng, B. Lu, C. Yu, C. Chuang, T.-I. Kim, T. Song, K. Shigeta, S. Kang, C. Dagdeviren, I. Petrov, P. V. Braun, Y. Huang, U. Paik, J. A. Rogers, Stretchable batteries with self-similar serpentine interconnects and integrated wireless recharging systems. *Nat. Commun.* **4**, 1543 (2013).

31. A. Lamoureux, K. Lee, M. Shlian, S. R. Forrest, M. Shtein, Dynamic kirigami structures for integrated solar tracking. *Nat. Commun.* **6**, 8092 (2015).
32. T. C. Shyu, P. F. Damasceno, P. M. Dodd, A. Lamoureux, L. Xu, M. Shlian, M. Shtein, S. C. Glotzer, N. A. Kotov, A kirigami approach to engineering elasticity in nanocomposites through patterned defects. *Nat. Mater.* **14**, 785–789 (2015).
33. Q. Hua, J. Sun, H. Liu, R. Bao, R. Yu, J. Zhai, C. Pan, Z. L. Wang, Skin-inspired highly stretchable and conformable matrix networks for multifunctional sensing. *Nat. Commun.* **9**, 244 (2018).
34. D. J. Lipomi, M. Vosgueritchian, B. C.-K. Tee, S. L. Hellstrom, J. A. Lee, C. H. Fox, Z. Bao, Skin-like pressure and strain sensors based on transparent elastic films of carbon nanotubes. *Nat. Nanotechnol.* **6**, 788–792 (2011).
35. C. M. Boutry, M. Negre, M. Jorda, O. Vardoulis, A. Chortos, O. Khatib, Z. Bao, A hierarchically patterned, bioinspired e-skin able to detect the direction of applied pressure for robotics. *Sci. Robot.* **3**, eaau6914 (2018).
36. M. S. Sarwar, Y. Dobashi, C. Preston, J. K. M. Wyss, S. Mirabbasi, J. D. W. Madden, Bend, stretch, and touch: Locating a finger on an actively deformed transparent sensor array. *Sci. Adv.* **3**, e1602200 (2017).
37. Y. Zang, F. Zhang, C. Di, D. Zhu, Advances of flexible pressure sensors toward artificial intelligence and health care applications. *Mater. Horiz.* **2**, 140–156 (2015).
38. J. Li, R. Bao, J. Tao, Y. Peng, C. Pan, Recent progress in flexible pressure sensor arrays: From design to applications. *J. Mater. Chem. C* **6**, 11878–11892 (2018).
39. J. Wu, Z. Wu, H. Xu, Q. Wu, C. Liu, B.-R. Yang, X. Gui, X. Xie, K. Tao, Y. Shen, J. Miaod, L. K. Norforde, An intrinsically stretchable humidity sensor based on anti-drying, self-healing and transparent organohydrogels. *Mater. Horiz.* **6**, 595–603 (2019).
40. H. Ota, K. Chen, Y. Lin, D. Kiriya, H. Shiraki, Z. Yu, T.-J. Ha, A. Javey, Highly deformable liquid-state heterojunction sensors. *Nat. Commun.* **5**, 5032 (2014).

Acknowledgments: We acknowledge A. Zamarayeva, J. Jan, and J. Ting for the helpful discussions. **Funding:** This work was supported, in part, by the Bakar Fellows Program, the NSF under grant no. 1610899, and FlexTech Alliance under grant no. AFOSR 42299. X.W. acknowledges the support from China Scholarship Council under grant no. 201706240083.
Author contributions: X.W. and A.C.A. designed the project. X.W. designed and conducted the experiments. M.A. conducted signal processing. Y.K., J.Z., and M.E.P. contributed to the characterization. C.L. and J.W.E. helped to design the research and contributed to the analysis of the data and discussions. X.W. wrote the manuscript, and all authors read and revised the manuscript. **Competing interests:** X.W. and A.C.A. are inventors on a patent application (provisional no. 62/939523) filed through the University of California, Berkeley. The other authors declare that they have no competing interests. **Data and materials availability:** All data needed to evaluate the conclusions in the paper are present in the paper and/or the Supplementary Materials. Additional data related to this paper may be requested from the authors.

Submitted 5 November 2019
Accepted 9 June 2020
Published 24 July 2020
10.1126/sciadv.aba1062

Citation: X. Wu, M. Ahmed, Y. Khan, M. E. Payne, J. Zhu, C. Lu, J. W. Evans, A. C. Arias, A potentiometric mechanotransduction mechanism for novel electronic skins. *Sci. Adv.* **6**, eaba1062 (2020).